Applied Catalysis B: Environmental 232 (2018) 348–354

Contents lists available at ScienceDirect

Applied Catalysis B: Environmental

journal homepage: www.elsevier.com/locate/apcatb

Single-atom silver-manganese nanocatalysts based on atom-economy design for reaction temperature-controlled selective hydrogenation of bioresources-derivable diethyl oxalate to ethyl glycolate and acetaldehyde diethyl acetal

Jie Ding[a,b,c], Maohong Fan[a,c,d,*], Qin Zhong[b,**], Armistead G. Russell[d]

[a] Department of Chemical and Petroleum Engineering, University of Wyoming, Laramie, WY, 82071, USA
[b] School of Chemical Engineering, Nanjing University of Science and Technology, Nanjing, Jiangsu, 210094, PR China
[c] School of Energy Resources, University of Wyoming, 1000 East University Avenue, Laramie, 82071, WY, USA
[d] School of Civil and Environmental Engineering, Georgia Institute of Technology, Mason Building, 790 Atlantic Drive, Atlanta, 30332, GA, USA

ARTICLE INFO

Keywords:
Catalytic hydrogenation
Single-atom catalysis
Silver-manganese catalysts
Biomass
Diethyl oxalate

ABSTRACT

The research was designed to synthesize novel single-atom silver-manganese nanocatalysts with a simple method for producing highly demanded ethyl glycolate (EGly) and acetaldehyde diethyl acetal (ADA) by hydrogenating bioresources-derivable diethyl oxalate (DEO) under different temperatures. DEO conversions achieved with the catalyst are 80–100%. 100% EGly or 97% ADA selectivity was produced by simply tuning reaction temperatures. The single-atom silver-manganese nanocatalysts were formed through the entrance of Ag atoms into the lattice tunnels of hollandite-type manganese oxide (HMO) under H_2 reduction at 200 °C. The excellent activities of the nanocatalysts are mainly ascribed to the activation of H_2 and desirable chemical adsorption of DEO and ethanol. The EGly was formed through the first order hydrogenation of DEO, while the ADA was obtained via the hydrogenation, dehydration and reaction. With the help of high-efficiency nanocatalysts, bioresources are promising raw materials for producing various high-value chemicals in environmentally responsible manners.

1. Introduction

Ethyl glycolate (EGly), as one of important chemicals, is widely used in the synthesis of ethylene glycol, glycolic acid, glycine, malonate, glyoxylate, polymers and etc [1,2] as well as used as green solvent in the organic synthesis [3]. A number of catalytic and non-catalytic procedures have been developed for the petroleum-based synthesis of EGly [4,5,6]. However, partial hydrogenation is difficult to control, which hinders its further applications in industry. Therefore, the development of a more efficient and practical hydrogenation-controlling catalyst remains a significant challenge in the modern chemical industry.

Acetaldehyde diethyl acetal (ADA) is extensively used in pharmaceutical intermediates, fragrances, food additives and solvents [6,7]. It has also been widely applied in the synthesis of cosmetics, fragrances, dyes, plastics, adhesives, paint, membranes and more [6,8,9]. Up until now, ADA was produced mainly by the reactions of petroleum-derived acetaldehyde and ethanol with the help of acid catalysts at temperature range of 25–75 °C [10,11]. However, these methods suffer from batch procedure, environmental unfriendly, energy intensive, difficult in separation and low yields. Thus, the development of a simple, environmentally benign, cost-effective and continuous method using efficient catalysts for the synthesis of EGly and ADA is of great significance.

Bioresources to various chemicals over nanocatalysts has attracted wide attention in recent years mainly due to the high efficiency and environmental friendly [12,13]. It contains biomass catalytic decomposition to syngas [14], CO oxidative coupling to esters [15,16] and hydrogenation of esters over nanocatalysts [17]. The last step is a reaction of industrial importance especially ethylene glycol (EG) productions from dimethyl oxalates (DMO) or diethyl oxalates (DEO) [15,18]. DEO is a safe, non-explosive as well as environmental friendly oxalate that can provide a better alternative in ester hydrogenation. However, hydrogenation of DEO easily produces EG [15,19], and the hydrogenation intermediate EGly cannot be realized via the same copper-based catalysts [20]. Furthermore, there are no reports of ADA production over copper-based catalysts via DEO hydrogenation to date, which is likely due to the easy conversion to alcohols. This study developed a single-atom silver-manganese (Ag-HMO) nanocatalyst, which was capable of accelerating temperature-controlled selective

* Corresponding author at: Department of Chemical and Petroleum Engineering, University of Wyoming, Laramie, Wyoming, 82071, USA.
** Corresponding author at: School of Chemical Engineering, Nanjing University of Science and Technology, Nanjing, Jiangsu, 210094, PR China.
E-mail addresses: mfan@uwyo.edu, mfan3@mail.gatech.edu (M. Fan), zq304@mail.njust.edu.cn (Q. Zhong).

https://doi.org/10.1016/j.apcatb.2018.03.058
Received 6 December 2017; Received in revised form 7 February 2018; Accepted 19 March 2018
Available online 26 March 2018
0926-3373/

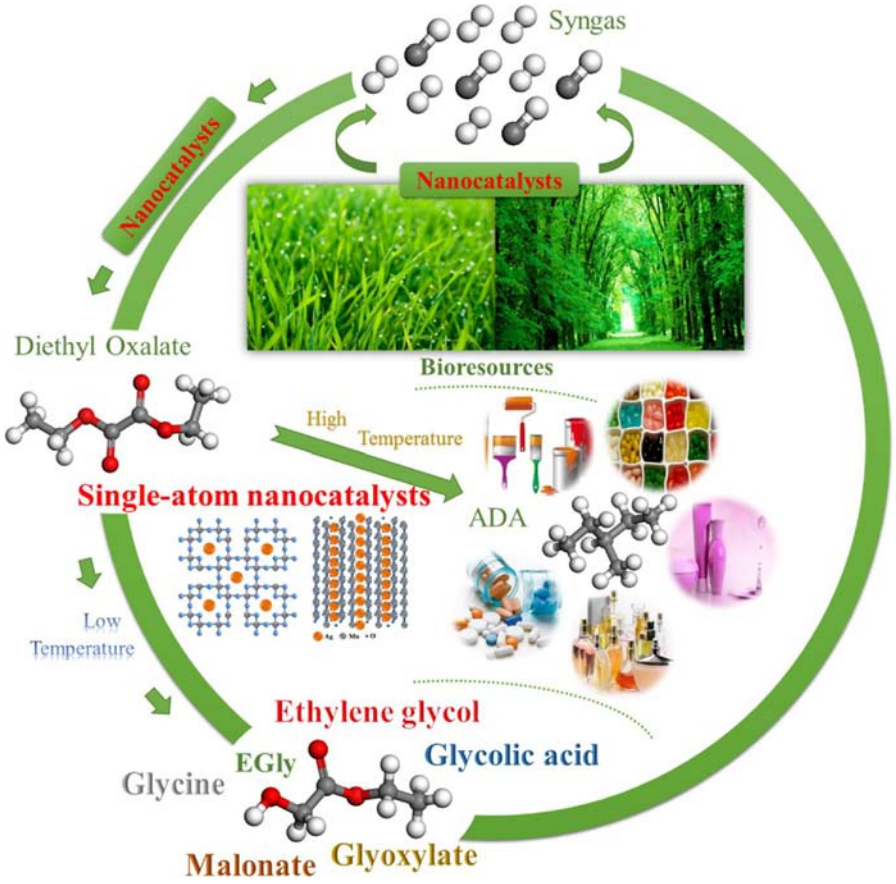

Fig. 1. The overall sketch from bioresources to various chemicals over nanocatalysts.

hydrogenation of DEO to EGly and ADA (Fig. 1). The findings have never been reported in literatures, although the single-atom catalysts and nanocatalysts have been widely applied in various fields [21,22].

2. Experimental sections

2.1. Catalyst preparations

The nanocatalysts were prepared, with certain modifications, according to the reported literatures [23,24]. For the synthesis of the Hollandite-type manganese oxide (HMO), 75 mL of a solution containing $MnSO_4{\cdot}H_2O$ (2.484 g) and $KMnO_4$ (1.659 g) was put into a 100 mL Teflon-lined stainless steel autoclave and heated to 160 °C for 24 h. The resulting black slurry was filtered and washed with deionized water, and then dried at 110 °C for 24 h. For the synthesis of Ag nanoparticles, ammonia (25 wt%) was added to a solution containing 0.945 g of $AgNO_3$ to form a transparent $[Ag(NH_3)_2]OH$ solution. Subsequently, the $[Ag(NH_3)_2]OH$ solution and H_2O_2 solution (30 wt%, 90 mL) were mixed and the precipitation was obtained by centrifuges. The Ag nanoparticles were obtained by drying at 80 °C for 24 h. For the synthesis of Ag decorated HMO (Ag-HMO), the $[Ag(NH_3)_2]OH$ and H_2O_2 solutions were added to the suspension (100 mL) containing the HMO (2.000 g) under stirring at 20 °C for 1 h. The final suspension was filtered and washed with distilled water, and then dried at 80 °C for 24 h to obtain the Ag-HMO.

2.2. Characterizations

The bulk composition was analyzed by inductively coupled plasma-atomic emission spectroscopy (ICP-AES; Thermo). The BET surface area was measured using N_2 physisorption at 77 K on an Autosorb IQ ASIQC0100-4 Quantachrome apparatus. The X-ray diffraction (XRD) patterns were collected on a Rigaku Smartlab XRD system using CuKα radiation (λ = 0.15418) at a scanning speed of 8°/min from 10° to 90° with 0.02° steps as well as 40 kV rube voltage and 40 mA current. The surface species were detected by a Kratos Axis Ultra DLD X-ray photoelectron spectrometer with a monochromated Al K-alpha source running at 150 W. Hydrogen temperature-programmed desorption (H_2-TPD) tests were performed on an Autosorb IQ ASIQC0100-4 quantachrome instrument equipped with a thermal conductivity detector (TCD). H_2-TPD was performed on catalysts after an initial 200 °C reduction in 95 vol.% H_2-5 vol.% N_2 for 6 h, after which adsorption was conducted at 40 °C with 100 vol.% H_2. Finally, desorption was programmed at 10 °C /min to 900 °C in flowing Ar. The morphology and size of the particles were observed by transmission electron microscopy (TEM) using Tecnai G2 F30 S-TWIN200 kV equipment. The FTIR spectra of the catalysts were recorded on a Nicolet IS50 FTIR spectrometer with a resolution of 4 cm^{-1}. In situ diffuse reflectance infrared Fourier transform spectroscopy (DRIFTS) measurements were performed on a Nicolet iS50 FTIR spectrometer (Thermo Scientific, Waltham, MA, USA) equipped with a DRIFS system with reaction chamber (Prqying Mantis model, Harrick Scientific Products, Pleasantville, NY, USA), employing ZnSe windows. UV–vis diffuse reflectance spectra (DRS) were obtained using a UV–vis spectrophotometer (Shimadzu UV-2550).

2.3. Catalytic activities

Catalytic activities were tested on a fixed bed reactor as previously reported [15]. Briefly, 500 mg of nanocatalysts were loaded into the center of the reaction tube (11 mm inner diameter and 500 mm length). The catalysts were reduced under 95% H_2/5% N_2 at 200 °C for 4 h at a

Table 1
Chemical and surface Ag compositions of Ag-HMO.

Samples	Bulk Ag content (wt%)	Surface Ag content (wt%)*
Fresh Ag-HMO	28.8	17.7
Reduced Ag-HMO	27.5	4.7

Note:
* means the data are from XPS analysis.

constant pressure. The temperature and the pressure were increased to the reaction temperature (220–420 °C) and the reaction pressure (2.9 MPa), respectively. The liquid 10% DEO/Ethanol (0.008 mL/min, Certified ACS > 99.8%, Sigma Aldrich) was pumped into the reactor. Gaseous products were analyzed by an online gas chromatograph SRI 8610 C equipped with two Restek-packed columns and a capillary column, while liquid products were collected and analyzed by an offline GC–MS Agilent 7890 A GC system-5975C VL MSD using an Agilent HP-5MS (30 m × 0.250 mm) capillary column equipped with automatic liquid sampler (ALS).

3. Results and discussions

3.1. Structural characterizations of Ag-HMO

The chemical and surface Ag compositions of fresh and reduced Ag-HMO were shown in Table 1. It can be found that the surface Ag content (17.7 wt%) was lower than the bulk Ag content (28.8 wt%) for the fresh Ag-HMO. It indicated that some of Ag species has entered into the lattice tunnels of HMO. However, the surface Ag content on the reduced Ag-HMO dramatically decreased, indicating that the reduction further promoted the entrance of Ag species into the lattice tunnels of HMO after reduction at 200 °C as reported in literature [23].

The HRTEM images were shown in Fig. 2a–f. The fresh Ag-HMO presented rod-like particles with large Ag aggregations on the surface of HMO (Figs. 2a and S1). The rod-like particles showed the lattice spacing of 0.694 nm, corresponding to the most stable [110] facets of HMO (Fig. 2b,c). The reduced Ag-HMO presented rod-like particles with much smaller Ag aggregations (Fig. 2d,e), which were consistent with the analysis of the chemical and surface Ag compositions of Ag-HMO. The HMO had 0.47 × 0.47 nm^2 square tunnels with a tetragonal prism, whose basic unit tunnel structure was built by eight (4 + 4) oxygen atoms with four sp^3-hybridized orbitals. Three oxygens in the tetragonal prism bonded to three Mn^{4+} cations and another occupied by long-pair electrons point to the central axis of the tunnel. Specially sized linear tunnels and electron-rich tunnel oxygen atoms could serve as a natural mold and an electron donor, respectively, which favored the formation of stable single-atom Ag chains in the lattice tunnels of the HMO. It has been reported that the Ag-HMO can be represented as $Ag_{1.8}Mn_8O_{16}$ when the lattice tunnels of HMO were completely occupied by Ag atoms [25]. The decrease of the Ag aggregations on the surface of HMO for the reduced Ag-HMO might be due to the entrance of Ag atoms into the lattice tunnels of HMO, and the apparent decrease of surface Ag compositions after reduction further confirmed the entrance of Ag atoms into the lattice tunnels of HMO. Fig. 2f showed that the silver atoms dispersed well in the lattice tunnels of the HMO for the reduced Ag-HMO, giving the appearance of “necklaces”. Each “pearl” represented one Ag atom (as indicated in Fig. S2). It was interesting that some of Ag atoms also entered into the lattice tunnels of HMO for the fresh Ag-HMO due to the lower contents of surface Ag species comparing with the bulk contents, while the Ag atoms were not observed in the lattice tunnels of HMO (Fig. 2c). It was possible that only few of Ag atoms entered into the lattice tunnels of HMO, which were difficult to be observed in the HMO.

The XRD patterns of fresh and reduced HMO and Ag-HMO were shown in Fig. 2g. The diffraction peaks of the fresh and reduced HMO matched well with the standard peaks of Hollandite [23], particularly the major peaks at 12.78°, 18.11°, 28.84°, 37.52° and 60.27° corresponding to the (110), (200), (310), (211) and (521) crystalline planes. It indicated that the fresh and reduced HMO presented hollandite type, and the 200 °C was not high enough to reduce the HMO in the H_2 atmosphere, which were consistent with the results of TEM images. The fresh Ag-HMO showed strong peaks at 38.18°, 44.41°, 64.55° and 77.40°corresponding to (111), (200), (220) and (311) planes of metallic Ag° with a weak peak at 33.20° corresponding to (200) plane of Ag_2O [26,27], indicating that the fresh Ag-HMO was composed by α-MnO_2, Ag_2O and metallic Ag°. The metallic Ag° in the fresh Ag-HMO was resulted from the single-atom Ag chains in the tunnels of the HMO reduced by the electron-rich tunnel oxygen atoms. The peaks corresponding to Ag_2O was disappeared in the reduced Ag-HMO, indicating that the Ag_2O was reduced by H_2 and the electron-rich tunnel oxygen atoms after reduction. Huang et al. has reported that the Ag atoms have the thermal migration properties [21,22]. The raise of the temperature during the reduction process promoted the Ag species to enter into the lattice tunnels of HMO and reduced by the electron-rich tunnel oxygen atoms. The Ag_2O remained on the surface of HMO was reduced by H_2 during the reduction process.

The chemical states were further investigated by XPS analysis. The Ag3d XPS was shown in Fig. 2h. The fresh Ag-HMO showed four peaks at ca. 368.1 eV and 374.1 eV with a spin-energy separation of 6.0 eV as well as ca. 367.6 eV and 373.5 eV with a spin-energy separation of 5.9 eV. The former two peaks were assigned to the Ag $3d_{3/2}$ and Ag $3d_{5/2}$ of Ag_2O, and the latter two peaks were attributed to the Ag $3d_{3/2}$ and Ag $3d_{5/2}$ of metallic Ag°, which agreed well with the previous reports [28,29]. It suggested that both metallic Ag° and Ag_2O existed in the fresh Ag-HMO. The reduced Ag-HMO showed only two peaks at 368.1 eV and 374.1 eV, indicating that there existed only metallic Ag° in the reduced Ag-HMO after reduction, which were consistent with the results of XRD patterns.

The Mn2p XPS of HMO and fresh/reduced Ag-HMO were shown in Fig. S3. The fresh and reduced HMO showed two distinct peaks with binding energies of 641.8 and 653.6 eV, and a spin-orbital splitting of 11.8 eV, were observed in the core level spectrum of fresh and reduced HMO. These values corresponded well to the Mn $2p_{3/2}$ and Mn $2p_{1/2}$ in MnO_2 [30,31], indicating that MnO_2 is the main components of Mn species in the fresh and reduced HMO, which were consistent with the results of XRD patterns and TEM images. The reduced Ag-HMO showed much higher binding energies, which was due to the strong interactions between Ag and HMO resulted from the entrance of Ag atoms into the lattice tunnels of HMO. Previous literatures have reported that the insertion of Ag atoms into the lattice tunnels of HMO lowering the bonding energies of Mn-O [21,22], and the electron density around Mn decreased, thus resulting in the increase of the binding energies of Mn2p XPS. The fresh Ag-HMO showed the peaks at the similar binding energies with the ones of HMO, this was because only few Ag atoms entered into the lattice tunnels of HMO and the interactions between Ag and HMO were very weak.

From the above analysis, the overall process were described as shown in Fig. 2i. The Ag were firstly loaded on the surface of HMO, and few of Ag species entered into the lattice tunnels of HMO. The reduction process further promoted the entrance of Ag atoms the lattice tunnels of the HMO for the formation of Ag atom sequences as shown in Fig. 2f. There existed HMO, Ag_2O and metallic Ag° on the surface for the fresh Ag-HMO, and the reduced Ag-HMO presented HMO and metallic Ag° on the catalyst surface.

3.2. Catalytic activities of Ag-HMO

The exploration of suitable reaction conditions was shown in Figs. S4 and S6, and the catalytic performance of Ag-HMO under different reaction temperatures is shown in Fig. 3. The DEO conversion increased rapidly with the reaction temperature rising. The HMO showed almost

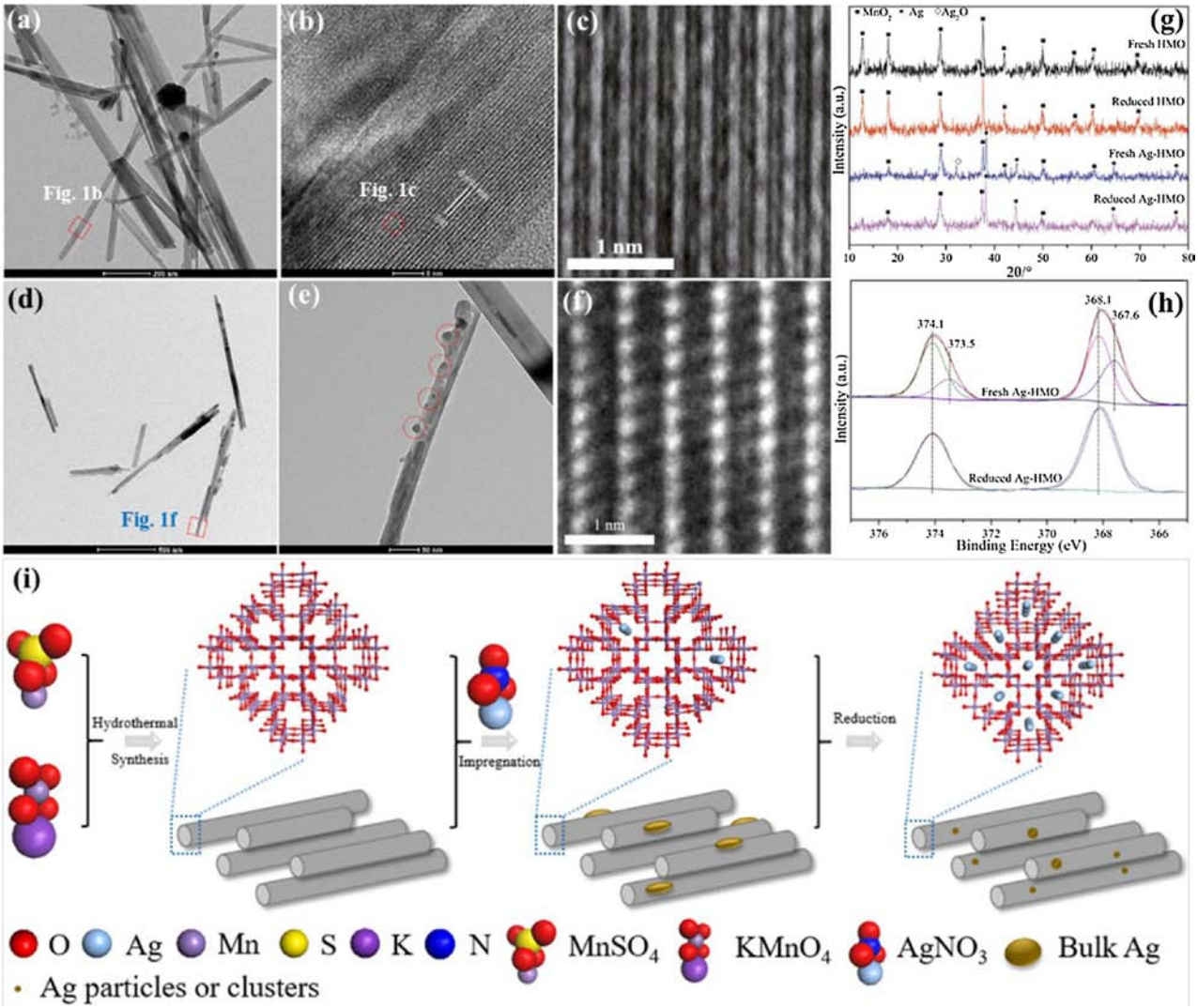

Fig. 2. Structures and formations of the single-atom Ag-HMO catalyst. HRTEM images of fresh Ag-HMO (a–c) and reduced Ag-HMO (d-f); (g) XRD patterns of fresh and reduced HMO and Ag-HMO; (h) Ag3d XPS of fresh and reduced Ag-HMO; (i) Formation mechanisms of Ag-HMO.

no EGly and ADA selectivity, while the ones were apparently increased on Ag-HMO. EGly was the dominant product at the low temperature, and the selectivity decreased with an increase in reaction temperature, which reached as high as 100% in the temperature range of 220 ~ 240 °C on the Ag-HMO. The ADA selectivity increased up to 100% at a reaction temperature of 390 °C and then remained constant with the reaction temperature rising. The Ag nanoparticles exhibited 0% EGly selectivity and 59% ADA selectivity. This indicated that Ag nanoparticles played an important role in the DEO conversion to ADA.

Long-term catalytic performances have been studied on Ag-HMO under 240 °C and 390 °C, respectively (Fig. 3d). The overall conversion of DEO and selectivity to EGly were stabilized at 90% and 82% at 240 °C, respectively. The Ag-HMO could also run stably at 390 °C with a full conversion of DEO and selectivity to ADA higher than 95% without any deactivations, even after 200 h of time on stream. The Ag-HMO demonstrated a long-term catalytic lifespan and catalytic active sites for EGly and ADA.

3.3. Catalytic mechanisms for EGly and ADA formations

Various characterizations were used for the analysis of the mechanisms. As shown in Figs. S8 and 4a, the generation of EGly was not changed while the ADA dramatically decreased when the ethanol was instead of acetone to dilute the DEO. The experiments without DEO also showed no ADA productions. As shown in Fig. 3a, the EGly selectivity started to gradually decrease while the ADA selectivity gradually increased with the reaction temperature rising. The EGly selectivity apparently decreased at the temperature of > 260 °C, while the ADA selectivity started to apparently increase until the reaction temperature reached > 310 °C. It illustrated that the formation of ADA was mainly from the reaction of DEO, H_2 and ethanol. The partial hydrogenation of DEO or dimethyl oxalate (DMO) over silver based catalysts has been widely reported previously [20,32–35]. Therefore, the formation mechanisms of ADA was detailed investigated in this research.

The DRIFTS with MS was used to analyze the reaction mechanisms. The DRIFTS of the reduced Ag-HMO were shown in Fig. 4b and the key peaks were enlarged in Fig. S12. As shown in Figs. 4b and S12, the bands at 2985 and 2902 cm^{-1} corresponding to the stretching vibrations of −OH in ethanol and the bands at 1750, 1572, 1395 cm^{-1} corresponding to the bending vibrations of -OH in ethanol were observed [36,37]. The band at 1759 cm^{-1} assigning to the C═O adsorption of oxalates was also observed [38,39].It should be noted that the peak at 1049 cm^{-1} corresponding to bending vibrations of -OH was observed at the reaction temperature < 360 °C, and it disappeared at the reaction temperature > 360 °C, while -OH bending vibrations of ethanol increased with the reaction temperature rising. It indicated that

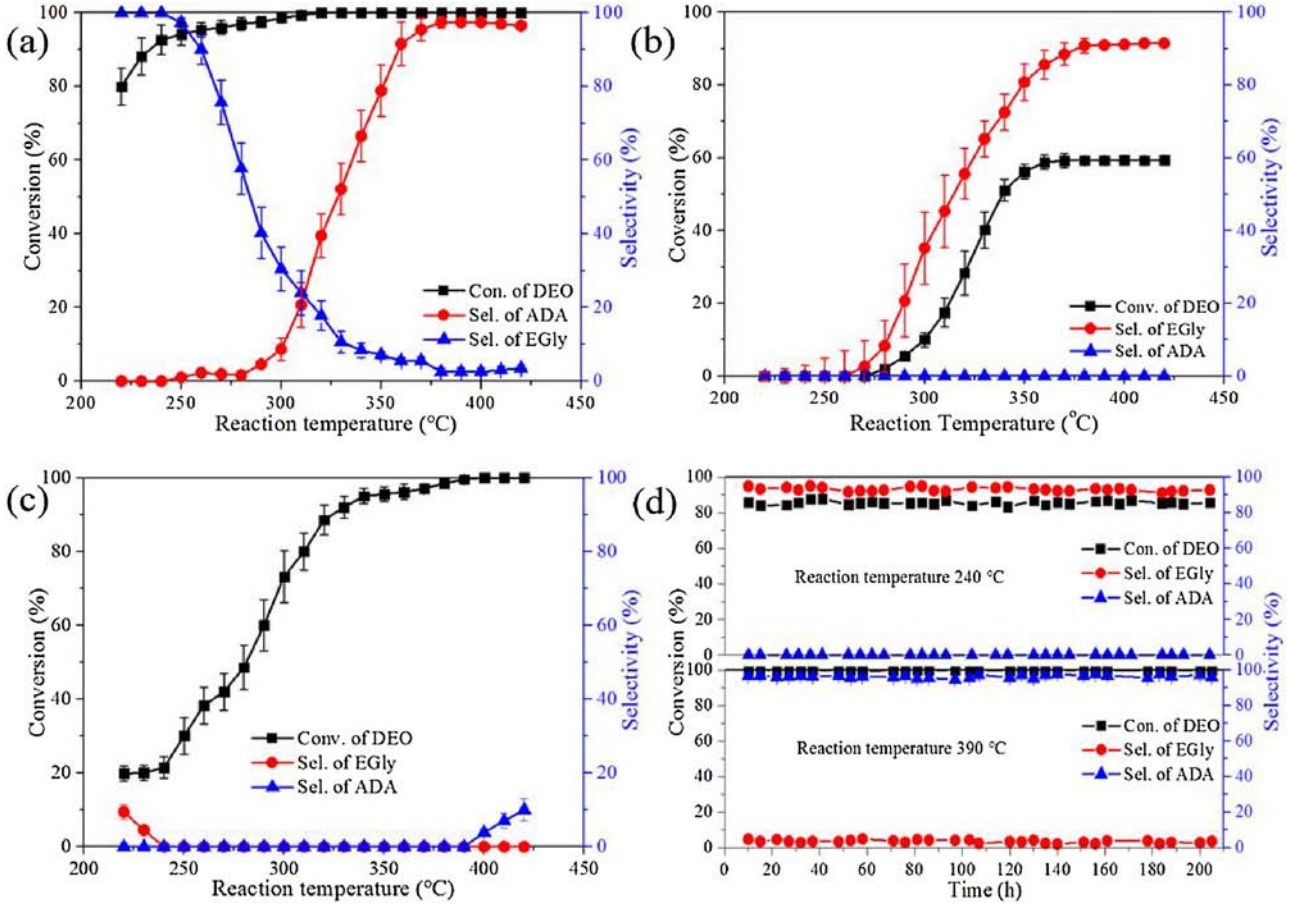

Fig. 3. Catalytic performance in hydrogenation of DEO. (a) Ag-HMO, (b) Ag nanoparticles, (c) HMO and (d) Catalytic stability of Ag-HMO.

the peak appeared at 1049 cm^{-1} at < 360 °C may be attributed to the -OH in EGly and EG. The GC—MS of liquid-phase productions in Fig. 4c showed that the EGly and EG were observed at < 360 °C, while they were disappeared over 360 °C, which further confirmed that the peak at 1049 cm^{-1} was attributed to the -OH vibrations of EGly or EG. The increase of the peak intensity of ethanol with the reaction temperature rising was due to the chemical adsorption of ethanol. When the reaction temperature reached 320 °C, the peak at 1116 cm^{-1} corresponding to C═O bending vibrations of acetaldehyde was observed [40,41]. The acetaldehyde was also observed in the MS of gas-phase productions at 320 °C as shown in Fig. 4d. The peaks at 1012 and 904 cm^{-1} corresponding to the vibrations of tertiary carbon group were appeared at the reaction temperature > 340 °C, which might be attributed to the generation of ADA, because the ADA contained tertiary carbon group. The ADA was also observed in the GC—MS of liquid-phase productions, further confirming the generation of ADA. Therefore, the reaction mechanisms can be deduced as shown in Fig. 4e. The DEO was firstly reacted with H_2 to form EGly and EG, and then the EG was dehydrated to acetaldehyde, and finally, the acetaldehyde was reacted with ethanol to form ADA. The production of ADA from acetaldehyde and ethanol has also been reported previously [8]. The oxalates hydrogenation was reported to be ceased at the step of EGly over silver-based catalysts at 220 °C as the literature reported [20,29–32]. It also has been reported that the EGly hydrogenated to EG at 280 °C [20] and the activation energy of EG dehydrogenation to acetaldehyde reached as high as 296.78 kJ/mol [42]. Such high activation energy required the high reaction temperature. Therefore, the EGly with high selectivity was obtained at the low temperature while the ADA was achieved at high temperature.

According to the above mechanisms, the chemical adsorptions of H_2, DEO and ethanol played an important role in the reactions. The H_2 adsorption-desorption properties of the reduced HMO, Ag nanoparticels (as shown in Fig. S13) and the reduced Ag-HMO were characterized by the H_2-TPD profiles as shown in Fig. 5a. It has been reported that the H_2 desorption peaks between 200 and 700 °C were attributed to the desorption of the chemisorbed H_2 [43,44]. The Ag nanoparticles showed almost no H_2 adsorption. The HMO and Ag-HMO exhibited a large peak at 691 °C and 236 °C, respectively, and both peaks were attributed to splitting H-H peaks [40,41]. This suggested that the HMO would chemisorb the H_2, while the Ag nanoparticles would not chemisorb the H_2. The single-atom Ag in the HMO tunnels might promote H_2 adsorption and dissociation on HMO at low temperatures, and also might be one of the main reasons for the high activity over Ag-HMO. To further confirm the relationship between the single-atom Ag and the H_2 activation, variations of peak areas of low-temperature H_2 with the silver loadings have been investigated as shown in Fig. S9. As the literature reported [21,22], the numbers of single-atom silver increased with the enhancement of silver loadings when the silver loadings were < 10 wt%. It could be found from Fig. S9 that there was a linear correlation between silver loadings and low-temperature activation H_2 when the silver loadings were < 10%. However, the low-temperature activation H_2 was not dramatically increased with the further increase of silver loadings. It indicated that the low-temperature activation H_2 was attributed to the single-atom silver. It may be caused by the decrease of the electron density around Mn resulted from the insertion of Ag atoms into HMO lattice tunnels.

In-situ DRIFTS for the adsorption of ethanol are shown in Fig. 5b. From the chat, both catalysts showed the bands appearing at 2985 and 2902 cm^{-1} corresponding to the stretching vibrations of —OH in ethanol, and the bands at 1750, 1395 and 1059 cm^{-1} attributed to the

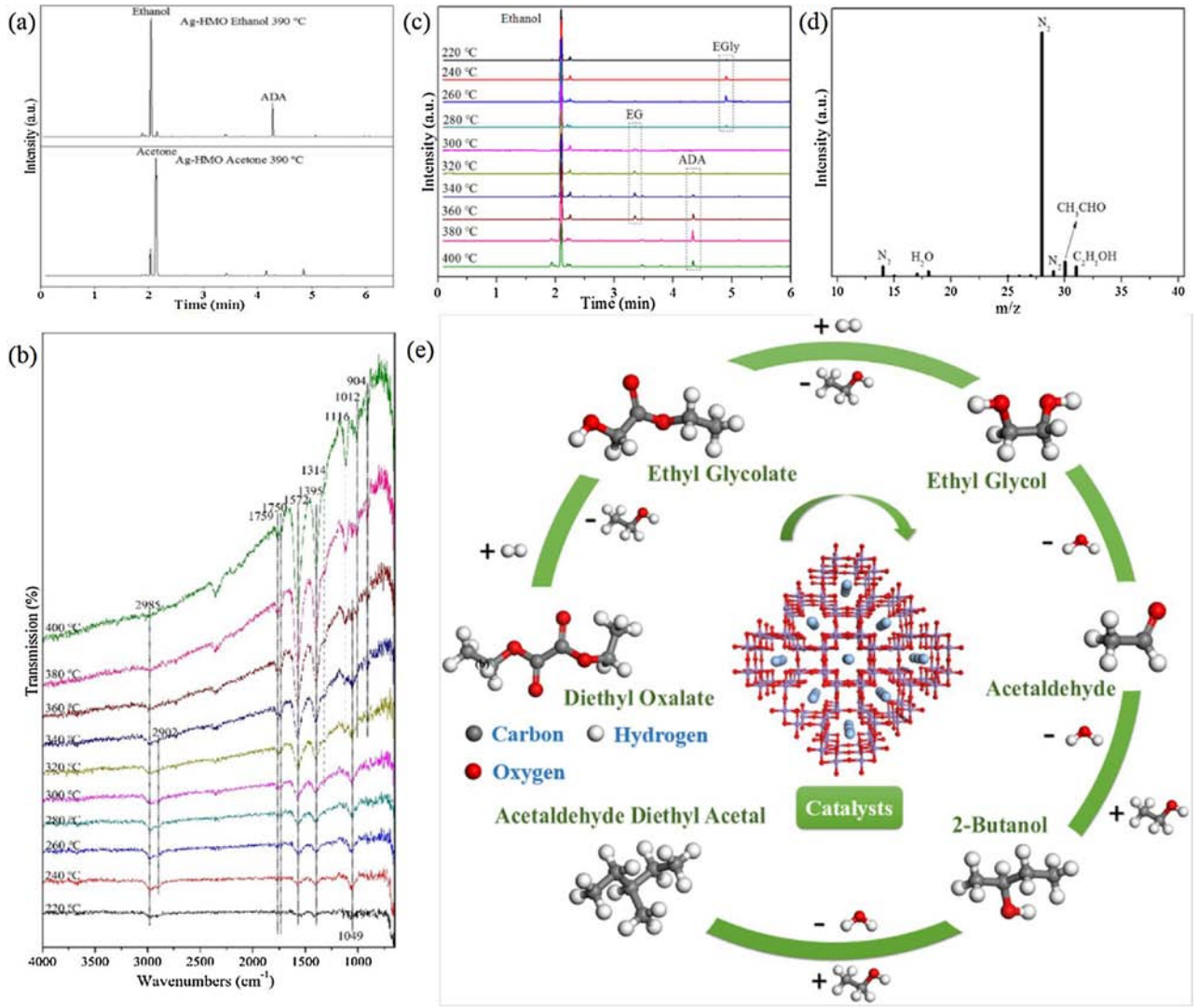

Fig. 4. (a) GC–MS spectra of products over Ag-HMO at 390 °C; (b) In-situ FTIR spectra of DEO over Ag-HMO; (c) GC–MS spectra of productions at different temperatures; (d) MS spectra of gas-phase productions at 320 °C; (f) Reaction mechanisms of DEO over Ag-HMO.

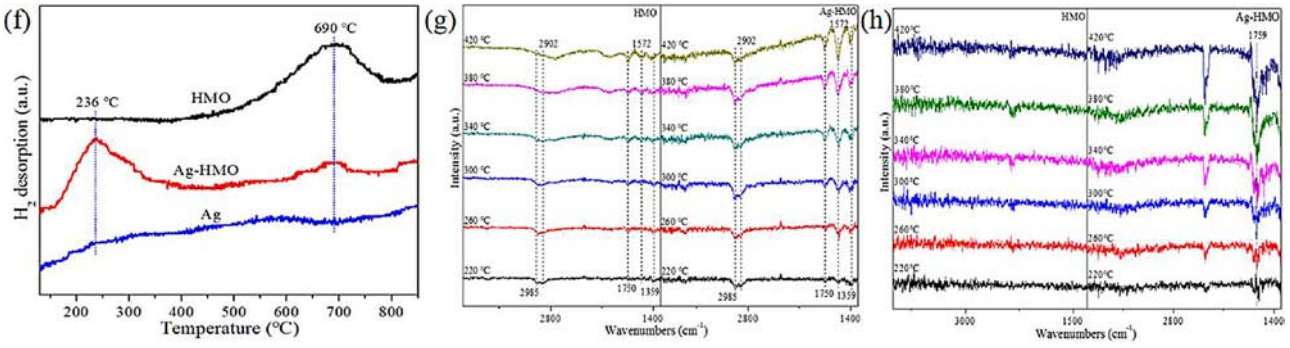

Fig. 5. (a) H2-TPD profiles of HMO, Ag-HMO and Ag nanoparticles; (b) In-situ FTIR of DEO adsorption over HMO and Ag-HMO; (c) In-situ FTIR of ethanol adsorption of HMO and Ag-HMO.

bending vibrations of −OH in ethanol. It can be seen that the HMO exhibited very weak ethanol adsorption, while the Ag-HMO showed much stronger adsorption peaks, suggesting that the Ag species played an important role in the adsorption of the ethanol. It has been reported that the Ag species might be the main adsorption sites for the organics [41,45].

The in situ DRIFTS for the adsorption of DEO are shown in Fig. 5c. From the chat, the band appearing at 1759 cm^{-1} was assigned to the C═O adsorption of oxalates [15,46]. The reduced Ag-HMO exhibited an apparent peak at 1759 cm^{-1}, and the peak increased with the temperature rising, indicating that the DEO was chemically adsorbed on the surface of the reduced Ag-HMO, while the reduced HMO exhibited almost no peaks, suggesting that the Ag species played an important role in the adsorption of the DEO.

Overall, it can be obtained from the above analysis that the single-atom Ag in the HMO lattice tunnels had a strong interaction with the HMO and promoted the Ag-HMO to chemisorb and activate the H_2 on the surface at the low temperature. The Ag species, mainly the metallic Ag° species, played an important role in the chemisorption of ethanol and DEO. The EG dehydration was one of critical procedures for the production of ADA, and the activation energy of EG dehydration reached as high as 296.78 kJ/mol. Therefore, the EGly with high selectivity was obtained at low temperature while the ADA was achieved at high temperature.

4. Conclusions

This study developed a novel synthetic route and high-efficiency Ag-HMO nanocatalysts for the production of EGly and ADA via hydrogenation of bioresources-derivable DEO. The high selectivity of EGly or ADA was obtained simply by regulating the reaction temperature via hydrogenation of DEO with robust activity and stability. The high performance of the nanocatalysts may be mainly ascribed to the strong chemical adsorptions of DEO, H_2 and ethanol, with the activation of H_2 resulting from the interactions between Ag and HMO. The single-atom silver inserted into the lattice tunnels of HMO promotes the adsorption and dissociation of H_2. The metallic Ag° on the surface of HMO adsorbed and activated the DEO and ethanol, thus promoting the production of EGly and ADA. The EG dehydration to acetaldehyde, one of the critical procedures for the ADA productions, required high activation energy and high temperature. Thus, the EGly with high selectivity was obtained at low temperature while the ADA was achieved at high temperature.

Acknowledgements

The first two departments contribute equally to this work. This work is financially supported by the U. S. Deparment of Energy, State of Wyoming and China Scholarship Council.

Appendix A. Supplementary data

Supplementary material related to this article can be found, in the online version, at doi:https://doi.org/10.1016/j.apcatb.2018.03.058.

References

[1] L. Mazzocchetti, M. Scandola, Z. Jiang, Z. Eur. Polym. J. 47 (2011) 942–948.
[2] S.A. Moore, D.E.G. Shuker, J. Label. Compd. Rad. 54 (2011) 855–858.
[3] R.D. Clercq, M. Dusselier, B.F. Sels, Green Chem. 19 (2017) 5012–5040.
[4] C. Ziebart, R. Jackstell, M. Beller, ChemCatChem 5 (2013) 3228–3231.
[5] X. Zheng, H. Lin, J. Zheng, X. Duan, Y. Yuan, ACS Catal. 3 (2013) 2738–2749.
[6] M. Pfreundschuh, D. Harder, Z. Ucurum, D. Fotiadis, D.J. Müller, Nano Lett. 17 (2017) 3261–3269.
[7] Y. Sasaki, T. Endo, N. Tanaka, H. Inoue, Green Chem. 11 (2009) 27–35.
[8] C. Lv, S. Pi, J. Chen, D. Lu, P. Ouyang, US patent 20140378711, 2015.
[9] Y. Okumura, H. Kouka, T. Aoki, US patent 20100261936, 2010.
[10] J. Shan, N. Janvelyan, H. Li, J. Liu, T.M. Egle, J. Ye, M.M. Biener, J. Biener, C.M. Friend, M. Flytzani-Stephanoupoulos, Appl. Catal. B 205 (2017) 541–550.
[11] X. He, H. Liu, Catal. Today 33 (2014) 133–139.
[12] X. Zhang, H. Lei, S. Chen, J. Wu, Green Chem. 18 (2016) 4145–4169.
[13] S. Song, L. Di, G. Wu, W. Dai, N. Guan, L. Li, Appl. Catal. B 205 (2017) 393–403.
[14] S. Zhao, S. Toan, S. Chen, W. Xiang, M. Fan, M. Zhu, S. Ma, Int. J. Hydrogen Energ. 42 (2017) 16031–16038.
[15] J. Ding, T. Popa, J. Tang, K. Gasem, M. Fan, Z. Qin, Appl. Catal. B 209 (2017) 530–542.
[16] T. Popa, Y. Zhang, E. Jin, M. Fan, Appl. Catal. A 505 (2015) 52–61.
[17] E. Jin, L. He, Y. Zhang, A.R. Richard, M. Fan, RSC Adv. 90 (2014) 48901–48904.
[18] S. Peng, Z. Xu, Q. Chen, Z.Wang D. Lv, J. Sun, Y. Chen, G. Guo, ACS Catal. 5 (2015) 4410–4417.
[19] J. Ding, J. Zhang, C. Zhang, K. Liu, H. Xiao, F. Kong, J. Chen, Appl. Catal. A. 508 (2015) 68–79.
[20] A. Yin, X. Guo, W. Dai, K. Fan, Chem. Commun. 46 (2010) 4348–4350.
[21] L. Zhu, X. Liu, H. Jiang, L. Sun, Chem. Rev. 117 (2017) 8129–8176.
[22] X. Yang, A. Wang, B. Qiao, J. Li, J. Liu, T. Zhang, Accouts Chem. Res. 46 (2013) 1740–1748.
[23] Z. Huang, X. Gu, Q. Cao, P. Hu, J. Hao, J. Li, X. Tang, Angew. Chem. Int. Ed. 124 (2012) 4274–4279.
[24] P. Hu, Z. Huang, Z. Amghouz, M.Makkee F. Xu, F. Kapteijn, A. Dikhtiarenko, Y. Chen, X. Gu, X. Tang, Angew. Chem. Int. Ed. 53 (2014) 3418–3421.
[25] M.C. Fung, M. Jasen, Angew. Chem. Int. Ed. 23 (1984) 906–907.
[26] J. Liu, R. Li, Y. Hu, T. Li, Z. Jia, Y. Wang, Y. Wang, X. Zhang, C. Fan, Appl. Catal. B 202 (2017) 64–71.
[27] J. Ding, Y. Bu, M. Ou, Y. Yu, Q. Zhong, M. Fan, Appl. Catal. B 202 (2017) 314–325.
[28] Y. Cui, Q. Ma, X. Deng, Q. Meng, X. Cheng, M. Xie, X. Li, Q. Cheng, H. Liu, Appl. Catal. B 206 (2017) 136–145.
[29] R. Das, S. Giri, A.L.K. Abia, B. Dhonge, A. Maity, A.C.S. Sustain, Chem. Eng. 5 (2017) 2711–2724.
[30] G. Cebello, R.A. Davoglio, Appl. Catal. B 218 (2017) 192–198.
[31] X. Han, C. Li, X. Liu, Q. Liu, Q. Xia, Y. Wang, Green Chem. 19 (2017) 996–1004.
[32] J. Zheng, X. Duan, H. Lin, Z. Gu, H. Fang, J. Li, Y. Yuan, Nanoscale 8 (2016) 5959–5967.
[33] J. Zhou, X. Duan, L. Ye, J. Zheng, M. Li, S.C.E. Tsang, Z. Yuan, Appl. Catal. A 505 (2015) 344–353.
[34] Y. Chen, L. Han, J. Zhu, P. Chen, S. Fan, G. Zhao, Y. Liu, Y. Lu, Catal. Comm. 96 (2017) 58–62.
[35] H. Chen, J. Tan, J. Cui, X. Yang, H. Zheng, Y. Zhu, Y. Li, Mol. Catal. 443 (2017) 346–352.
[36] W.J. Pech-Rodriguez, D. Gonzalez-Quijano, G. Vargas-Gutierrez, C. Morais, T.W. Napporn, F.J. Rodriguez-Varela, Appl. Catal. B 203 (2017) (2017) 654-332.
[37] A.B. Delpeuch, F. Maillard, M. Chatenet, P. Soudant, C. Cremers, Appl. Catal. B 181 (2016) 672–680.
[38] A. Situm, M.A. Rahman, N. Allen, N. Kabengi, H.A. Al-Abadleh, J. Phys. Phys. Chem. 121 (2017) 5569–5579.
[39] L. Mino, A. Zecchina, G. Martra, A.M. Rossi, G. Spoto, Appl. Catal. B 196 (2016) (2016) 135–141.
[40] C.A. Gierczak, L.L. Kralik, A. Mauti, A.L. Harwell, M.M. Maricq, Atmos. Environ. 150 (2017) 425–433.
[41] S. Maity, R.I. Kaiser, B.M. Jones, Phys. Chem. Chem. Phys. 17 (2015) 3081–3114.
[42] W.B. Smith, Tetrahedron 58 (2002) 2091–2094.
[43] Y.I. Hasegawa, R.U. Maki, M. Sano, T. Miyake, Appl. Catal. A 371 (2009) 67–72.
[44] Y. Zhang, L. Ma, T. Wang, X. Li, Fuel 177 (2016) 197–205.
[45] G. Xu, J. Ma, G. He, Y. Yu, H. He, Appl. Catal. B 207 (2017) 60–71.
[46] Z. Lin, S. Liu, J. Li, J. Chen, M. Xie, X. Li, M. Zhang, Q. Zhu, D. Huo, X. Sun, Mater. Des. 108 (2016) 640–647.